NEOPLASIA
www.neoplasia.com

Volume 10 Number 7 July 2008 pp. 727–735 727

Temporal Heterogeneity in Blood Supply in Human Tumor Xenografts[1,2]

Kjetil G. Brurberg, Jon-Vidar Gaustad, Camilla S. Mollatt and Einar K. Rofstad

Group of Radiation Biology and Tumor Physiology, Department of Radiation Biology, Institute for Cancer Research, Norwegian Radium Hospital, Montebello, Oslo, Norway

Abstract

Temporal heterogeneities in tumor blood supply were studied by using a recently developed first-pass imaging technique. First-pass imaging movies of A-07-GFP human tumor xenografts growing in window chambers were recorded at a frame rate of ~9 fps and a spatial resolution of $10.8 \times 10.8\,\mu m^2$ after a bolus of 155-kDa tetramethylrhodamine isothiocyanate–labeled dextran had been administered intravenously. Each tumor was subjected to imaging thrice, with 20 minutes between each repetition. Highly specific maps of the vascular network and blood supply time (BST) images (i.e., images of the time from when arterial blood enters a tumor through the main supplying artery until it reaches a vessel segment within the tumor) were produced from the movies. The tumors had one to three supplying arterioles and showed substantial temporal heterogeneity in BST. Homogeneous changes in BST in the entire vascular network were seen in tumors supplied by one arteriole. Blood supply time fluctuations in tumor subregions were observed in tumors having two or three supplying arterioles. In addition, individual vessel segments frequently showed significant changes in BST with time. High-magnification transmission microscopy imaging substantiated that BST changes could be a consequence of arterial/arteriolar vasomotor activity, vessel wall compression, varying flow rate, and vascular stasis.

Neoplasia (2008) 10, 727–735

Introduction

Human cells generally depend on an adequate supply of oxygen and nutrients to survive, and complex vascular networks are generated to fulfill this fundamental need. Normal tissues are characterized by a redundant arteriolar supply, with the blood flowing successively from arterioles covered by circumferential smooth muscle cells to venules and veins through well-defined capillary networks. Consequently, the blood supply of normal tissues is strictly regulated, ensuring a continuous and adequate supply of oxygen and nutrients to every cell in the parenchyma.

Most tumors are characterized by impaired blood supply caused by a combination of limited arteriolar supply, absent vessel hierarchy, and severe morphologic abnormalities such as contour irregularities, tortuous and elongated vessel segments, and arteriovenous shunts [1,2]. As a direct consequence of poor arteriolar supply and elongated vessel segments, erythrocytes may be depleted of oxygen on their way through the vascular network and give rise to longitudinal P_{O_2} gradients [1,3]. The chaotic microvascular architecture greatly increases the risk of vascular cessations, unstable blood flow, and development of acute hypoxia [4–7]. Consequently, blood flow heterogeneities may play an important role in the development of a hostile microenvironment in tumors.

Despite their potential importance, spatial and temporal heterogeneities in tumor blood supply have not been the subject of detailed, comprehensive investigations thus far, probably reflecting a lack of simple and adequate experimental methods. In the present study, we subjected window chamber preparations of tumors to blood supply time (BST) imaging [7]. Blood supply time values, representing the time from when arterial blood enters a tumor-supplying artery

Abbreviations: BST, blood supply time; GFP, green fluorescence protein; ROI, region of interest; TRITC, tetramethylrhodamine isothiocyanate

Address all correspondence to: Einar K. Rofstad, PhD, Department of Radiation Biology, Institute for Cancer Research, Norwegian Radium Hospital, Montebello, N-0310 Oslo, Norway. E-mail: einar.k.rofstad@rr-research.no

[1]**Grant Support:** This work was supported by the Norwegian Cancer Society.
[2]**Supplementary Material:** Supplementary movies 1 and 2 can be found at: http://radium.no/rofstad/?k=rofstad/Supplementary%20Material&aid=6432.
Received 15 March 2008; Revised 9 April 2008; Accepted 9 April 2008

DOI 10.1593/neo.08388

until it reaches a downstream vessel segment, were assigned to all vessels within a tumor cross section. This procedure was performed thrice for each tumor, enabling direct visualization of the spatial heterogeneity in blood supply and changes in this heterogeneity with time. Simultaneously, individual tumor-supplying arteries and tumor arterioles, microvessel segments, and venules were subjected to detailed investigations in an attempt to reveal biologic mechanisms provoking instabilities in tumor blood flow.

Materials and Methods

Tumor Model

A cutaneous window chamber was surgically implanted in the dorsal skin fold of adult (8–10 weeks of age) female BALB/c *nu/nu* mice by using a procedure similar to that reported earlier [7,8]. Briefly, a circular incision (ø ~ 6 mm) was made in the left skin layer, and the fascial surface of the right skin layer was exposed. The incision site was sandwiched by two parallel chamber frames, and an A-07-GFP human melanoma multicellular spheroid (ø ~ 0.1 mm) was implanted onto the fascial surface of the right skin layer [7,9]. Finally, the surgical site of the skin fold was covered by a plastic window. After surgery, the mice were housed in a Scantainer (Scanbur, Nittedal, Norway) maintained at a temperature of 30 to 32°C and 60% humidity with continuous access to sterilized food and tap water. Tumors with a diameter of 2 to 3 mm were subjected to intravital microscopy studies within 9 to 12 days after implantation. Animal care and experimental procedures were in accordance with the Interdisciplinary Principles and Guidelines for the Use of Animals in Research, Marketing, and Education (New York Academy of Sciences, New York, NY).

Anesthesia

Window chamber implantation and intravital microscopy were carried out with anesthetized mice. Fentanyl citrate (Janssen Pharmaceutica, Beerse, Belgium), fluanisone (Janssen Pharmaceutica), and midazolam (Hoffmann-La Roche, Basel, Switzerland) were administered IP in doses of 0.63, 20, and 10 mg/kg, respectively. After surgery, the mice were given buprenorphine (Temgesic; Schering-Plough, Brussels, Belgium) IP in a dose of 0.12 mg/kg. During surgery, the body core temperature of the mice was maintained between 37 and 38°C by using a heating pad, whereas a thermostatically controlled hot air generator was used to maintain the temperature during intravital microscopy.

First-Pass Imaging

During imaging, the mice were kept in a specially constructed holder that fixed the window chamber to the microscope stage. Imaging was performed by using an inverted fluorescence microscope equipped with filters for green and red lights (Model IX-71; Olympus, Munich, Germany), a ×1.25 objective lens, a black and white CCD camera (Model C4742-95; Hamamatsu Photonics, Hamamatsu, Japan), and appropriate image acquisition software (Wasabi; Hamamatsu Photonics). The spatial resolution was $10.8 \times 10.8\ \mu m^2$, and the field of view ($6.89 \times 5.51\ mm^2$) was adjusted to include both the tumor and the surrounding normal tissue. Fluctuations in blood supply were studied by repeated first-pass imaging of five tumors [7]. Briefly, 4 mg of tetramethylrhodamine isothiocyanate (TRITC)–dextran with a molecular mass of 155 kDa (Sigma-Aldrich, St. Louis, MO) was diluted in saline and administered into the lateral tail vein in a bolus dose of 0.05 ml. Simultaneously, epifluorescence images were acquired at a frame rate of ~9 fps and stored to a local computer. The imaging procedure was carried out thrice for each tumor, with 20 minutes between each recording.

Image Processing

Two-dimensional projected vascular masks were established from stored images as described elsewhere [7]. A total of three masks were derived for each tumor, one from each of the three imaging series. The masks were controlled for consistency before they were subjected to image fusion. Finally, three BST images were produced for each tumor by assigning a BST value to each pixel in the fused vascular mask [7]. The BST of a pixel was defined as the time difference between the frame showing maximum fluorescence intensity in the pixel and the frame showing maximum fluorescence intensity in the reference tumor-supplying artery. The velocity of the plasma flow in the reference artery was measured as described earlier [7].

Transmission Microscopy Imaging

To search for mechanisms behind temporal heterogeneities in tumor blood supply, window chamber preparations were subjected to high-magnification transmission microscopy imaging [7]. Individual tumor-supplying arteries and tumor arterioles, microvessels, and venules were imaged at a magnification of ×20, providing a spatial resolution of $0.67 \times 0.67\ \mu m^2$.

Statistical Analysis

Sigmoidal curves were fitted to cumulative plots of normalized BST distributions by regression analysis. Two parameters were derived from the regression analysis: median BST and the derivative of the cumulative plot at median BST. The latter parameter describes the intratumor heterogeneity in BST. It was assumed that these parameters followed a normal distribution with unknown variance. By using the Student's *t* distribution with 39 degrees of freedom, 99% confidence intervals were calculated for each of the parameters. Two BST frequency distributions were considered to be significantly different when the 99% confidence intervals did not overlap.

Results

Figure 1 shows background-subtracted fluorescence intensity courses for five single-pixel regions of interest (ROIs) in the vascular network of a representative window chamber preparation. The ROIs refer to the reference vessel (ROI 1) and four vessels (ROIs 2–5) in different tumor locations (Figure 1*A*). The fluorescence intensity courses were recorded after the first (Figure 1*B*), the second (Figure 1*C*), and the third (Figure 1*D*) injections of TRITC-dextran. Generally, the vessels showed fluorescence intensity courses with a well-defined peak, and the peak for pixels localized within the tumor vasculature was right-shifted relative to that for the pixels of the reference vessel. Because the vessels were leaky, the background intensity increased for each administration of contrast. However, alterations in the leakiness from one contrast administration to the next were not observed. Most importantly, the specificity of the intensity curves was not compromised by the leakiness of the vessels, and therefore, the position of the intensity peak could be determined accurately throughout the tumor vasculature in all three imaging series.

Consecutive measurements of BST may give different values, either because of changes in the blood supply between the measurements or because of poor experimental reproducibility. The reproducibility of our measurements seemed to be good, both at the single-pixel level

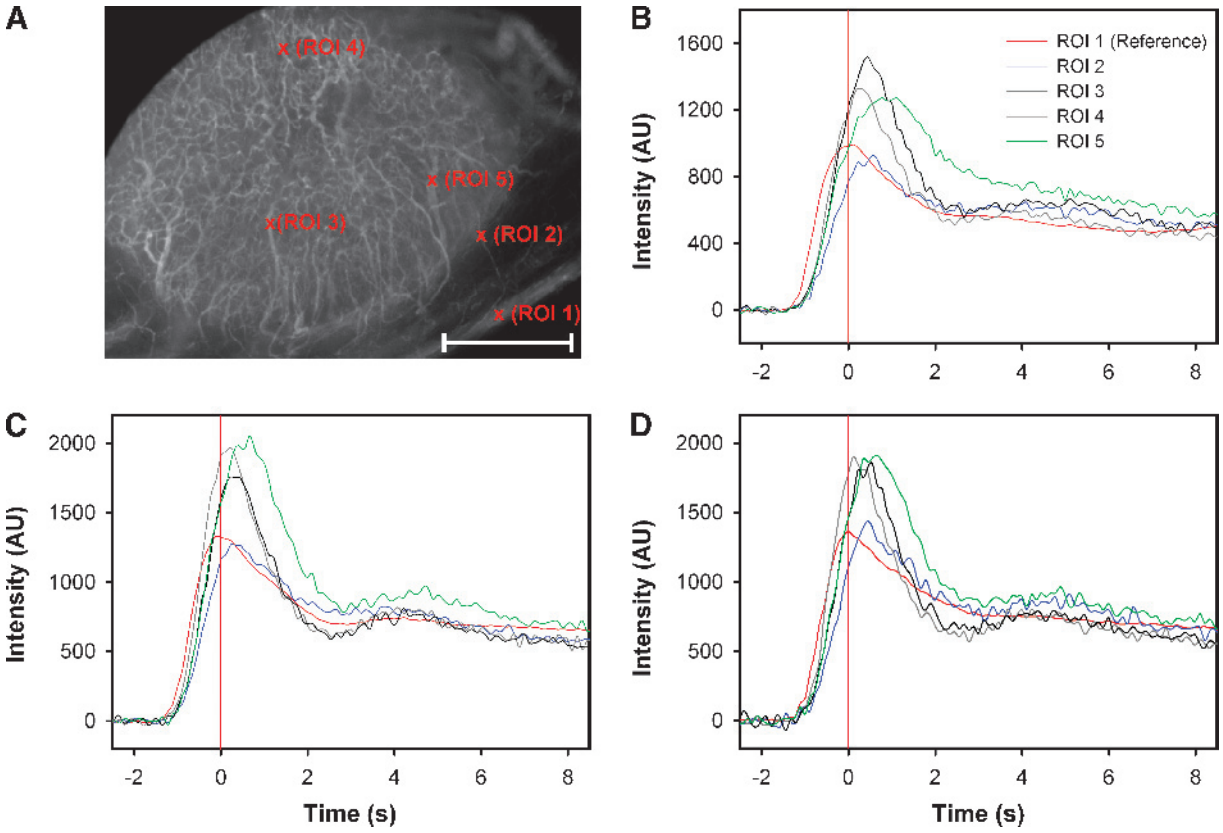

Figure 1. (A) The vascular network of an A-07-GFP window chamber tumor subjected to BST imaging thrice. Five single-pixel ROIs, representing the reference vessel (ROI 1) and four tumor vessels (ROIs 2–5), are indicated in the image. Scale bar, 1 mm. (B–D) Background-subtracted fluorescence intensity *versus* time curves for the five ROIs indicated in the image. The curves refer to the first (B), second (C), and third (D) injections of contrast. *Red vertical lines* indicate the point of time when the fluorescence intensity in the reference vessel was highest (i.e., BST = 0.0 second).

(Figure 1) and at the tumor level (Figure 2). Figure 2 refers to two representative tumors and shows BST frequency distributions recorded after a first (Figure 2*A*) and a second (Figure 2*B*) injection of TRITC-dextran. In both measurements, the median BST values of the tumors were 0.56 and 0.67 second, respectively. Statistical analysis showed that the BST frequency distributions of the two tumors differed significantly in median BST and heterogeneity in BST in both imaging series ($P < .01$), whereas the BST frequency distributions derived from the first and the second imaging series were not significantly different for any of the tumors ($P > .05$). The reproducibility of the measurements was examined further by subjecting the BST frequency distributions to pixel-by-pixel subtraction. Both tumors showed symmetrical ΔBST frequency distributions with median values of 0.0 second (Figure 2*C*).

Fluctuations in tumor blood supply were studied by subjecting five tumors to BST imaging thrice. The median value and the 25/75 percentiles of the BST frequency distributions derived from each of the three imaging series are shown in Figure 3*A*. The BST frequency distributions of tumors 2 to 5 did not change from one imaging series to the next, whereas median BST of tumor 1 decreased from 0.78 to 0.56 second during the first 20 minutes of the observation period, and then decreased further to 0.44 second during the following 20-minute interval. To examine the quality of the experiment, we investigated whether the physiological conditions of the mice had changed between the imaging series by measuring the plasma flow velocity in the reference vessel. The plasma flow velocity was found to be 15 to 16 μm/msec for all tumors, and it did not differ among the imaging series. More particularly, it was verified that the decrease in median BST with time of tumor 1 was not a consequence of physiological changes in the host mouse, because the plasma flow velocity in the reference vessel in the three imaging series was 15.5, 15.1, and 15.9 μm/msec, respectively. The quality of the BST measurements was examined further by pooling the ΔBST values obtained by subtracting the BST values of imaging series 1 from those of imaging series 2 and those obtained by subtracting the BST values of imaging series 2 from those of imaging series 3, and plotting the data as cumulative ΔBST frequency distributions (Figure 3*B*). In tumors 2 to 5, median ΔBST was close to 0.0 second, implying that the number of pixels in which BST increased from one imaging series to the next was approximately equal to the number of pixels in which BST decreased. Thus, in general, the BST measurements complied with the fact that increases and decreases in BST have to occur at similar frequencies.

Intertumor differences in BST were searched for by pooling the data from the three repeated BST measurements and plotting the data as cumulative BST frequency distributions (Figure 3*C*). The BST frequency distributions were shifted in time relative to each other, implying that the tumors differed in median BST. Thus, median BST was significantly higher for tumor 4 than for tumors 1, 2, 3, and 5 ($P < .01$), significantly higher for tumor 5 than for tumors 1, 2, and 3 ($P < .01$), and significantly higher for tumor 2 than for tumors 1 and

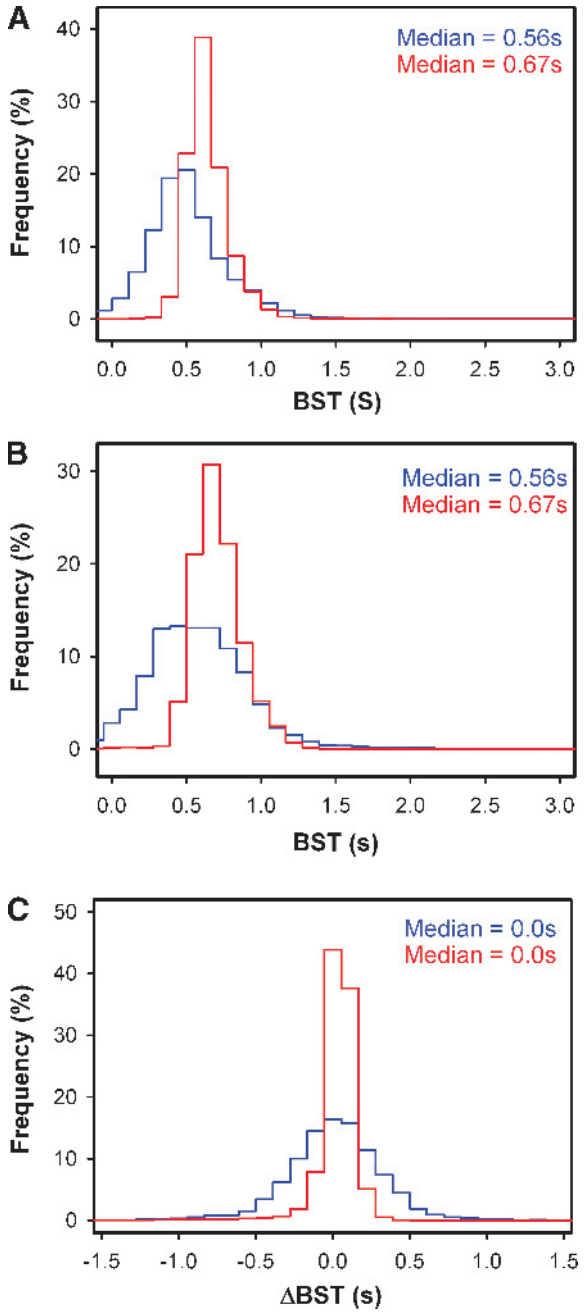

Figure 2. Two A-07-GFP window chamber tumors were subjected to BST imaging twice. (A) The BST frequency distributions of the tumors derived from the first imaging series. (B) The BST frequency distributions of the tumors derived from the second imaging series. (C) The ΔBST frequency distributions of the tumors, produced by pixel-by-pixel subtraction.

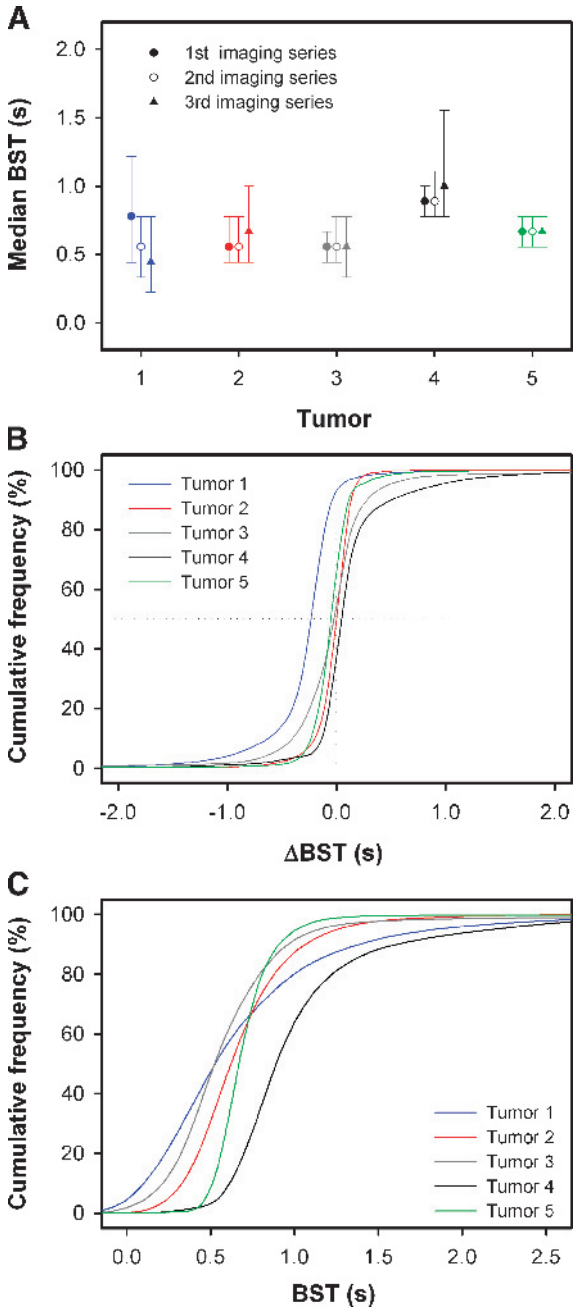

Figure 3. Five A-07-GFP window chamber tumors were subjected to BST imaging thrice. (A) Median BST and the 25/75 percentiles of the BST frequency distributions derived from each of the three imaging series. (B) Cumulative plots of the ΔBST frequency distributions of the five tumors. The ΔBST frequency distributions were obtained by pooling the ΔBST values obtained by subtracting the BST values of imaging series 1 from those of imaging series 2 and those obtained by subtracting the BST values of imaging series 2 from those of imaging series 3. (C) Cumulative plots of the BST frequency distributions of the five tumors. The BST frequency distributions were obtained by pooling the BST values derived from each of the three imaging series. The cumulative plots were based on 2×10^4 to 4×10^4 ΔBST (B) or BST (C) values. Sigmoidal curves were fitted to the data by regression analysis.

3 ($P < .01$). Moreover, the slope of the curves differed among the tumors, implying that the intratumor heterogeneity in BST varied from one tumor to the next. Thus, the intratumor heterogeneity in BST was significantly higher for tumor 1 than for tumors 2 to 5 ($P < .01$) and significantly lower for tumor 5 than for tumors 1 to 4 ($P < .01$).

Examination of the BST images derived from the triple imaging experiment revealed that the spatial heterogeneity in BST differed among the tumors. All tumors showed BST hot spots (i.e., tumor subregions with very low BST values). The hot spots appeared in the same tumor region in all three BST images, but the number of hot spots differed

among the tumors from 1 to 3. This is illustrated in Figure 4, which shows two BST images of a tumor having one hot spot (Figure 4*A*), a tumor having two hot spots (Figure 4*B*), and a tumor having three hot spots (Figure 4*C*). These hot spots delineated the initial blood supply to the tumors, and consequently, the number of hot spots reflected the number of tumor-supplying arterioles and their location within the tumors.

The BST data derived from the triple imaging experiment were subjected to detailed examination to investigate whether the tumors showed temporal heterogeneity in BST. In Figure 5, each of the five tumors is represented with two subsequent BST images (Figure 5*A*) and the corresponding ΔBST image (Figure 5*B*) and ΔBST frequency distribution (Figure 5*C*). For illustrative purposes, the reference vessel is included in the BST images and the ΔBST image of tumor 1 (*arrow 1*). The BST of the reference vessel is defined to be 0.0 second, and consequently, this vessel appears pink in the BST images and yellow in the ΔBST image. Examination of the BST images showed that BST changed gradually along tumor vessel segments without discontinuities in its numerical value. More interestingly, the BST images revealed substantial temporal heterogeneity in the blood supply of the tumors. The BST of tumor 1 decreased in the entire tumor between the imaging series, and the decrease was most clearly expressed in the periphery of the tumor (*arrow 2*). The blood supply of tumor 2 was fairly stable. Thus, almost all vessel segments have the same color in the two images, even in tumor regions showing significant BST heterogeneity (*arrow 1*). However, a few individual vessel segments localized in the upper left of the tumor underwent a shift toward lower BST values (*arrow 2*). Tumor 3 showed significant instabilities in BST. The area of the early perfused region in the upper part of the tumor increased slightly between the imaging series, implying that BST decreased in this region (*arrow 1*). Simultaneously, BST increased substantially in another early perfused region localized in the opposite half of the tumor (*arrow 2*). The microvasculature surrounding these two tumor regions did not undergo significant changes in BST. In tumor 4, BST did not change significantly between the imaging series in large tissue regions. However, a few individual vessels, mainly draining venules, showed slightly increased BST values with time (*arrow 1*). Tumor 5 showed extensive temporal heterogeneity in BST, with a large number of vessels changing from low to high BST values and *vice versa*. It should be noticed, however, that the magnitude of the changes was relatively modest. Moreover, as can be seen from the ΔBST image, vessels localized within the same subregion of the tumor showed coordinated changes in BST. Taken together, the three imaging series showed that temporal heterogeneity in BST can occur at three different levels in tumors: 1) individual vessels (i.e., microvessels and draining venules) can show changes in BST independent of each other, 2) vessels in tumor subregions can show coordinated fluctuations in BST, and 3) whole tumors can show coordinated and homogeneous

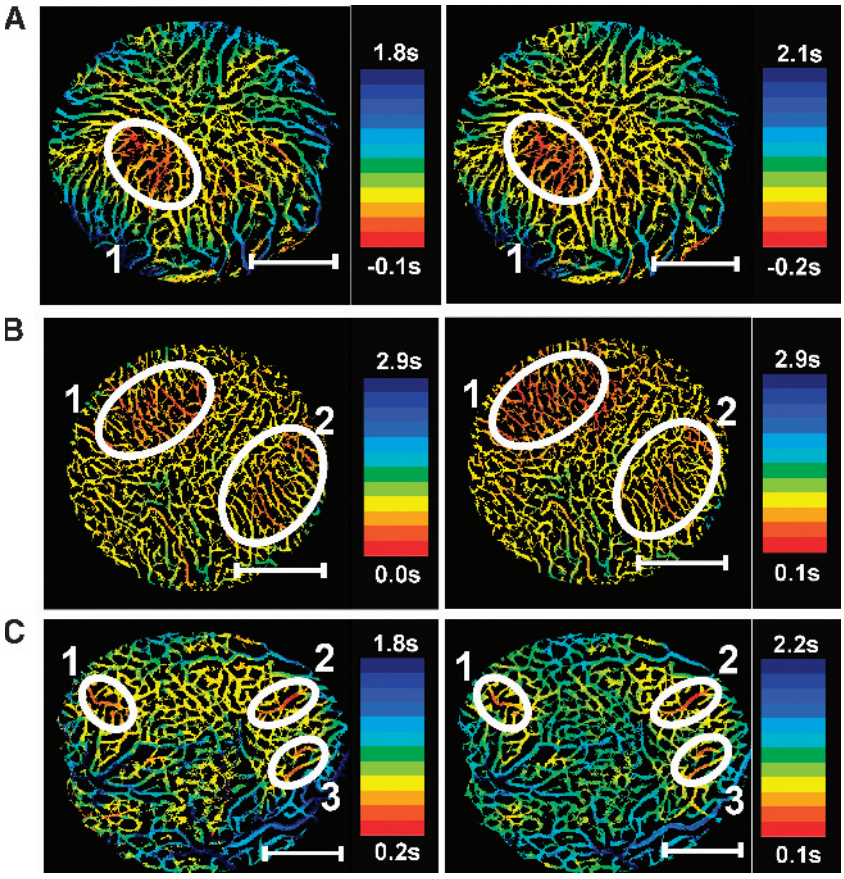

Figure 4. Five A-07-GFP window chamber tumors were subjected to BST imaging thrice. Three of the tumors are represented with two BST images each, illustrating that A-07-GFP tumors can have one (A), two (B), or three (C) BST hot spots, and hence, one, two, or three supplying arterioles. The color scales were adjusted individually in the BST images to highlight the hot spots. The hot spots are surrounded by white ellipses.

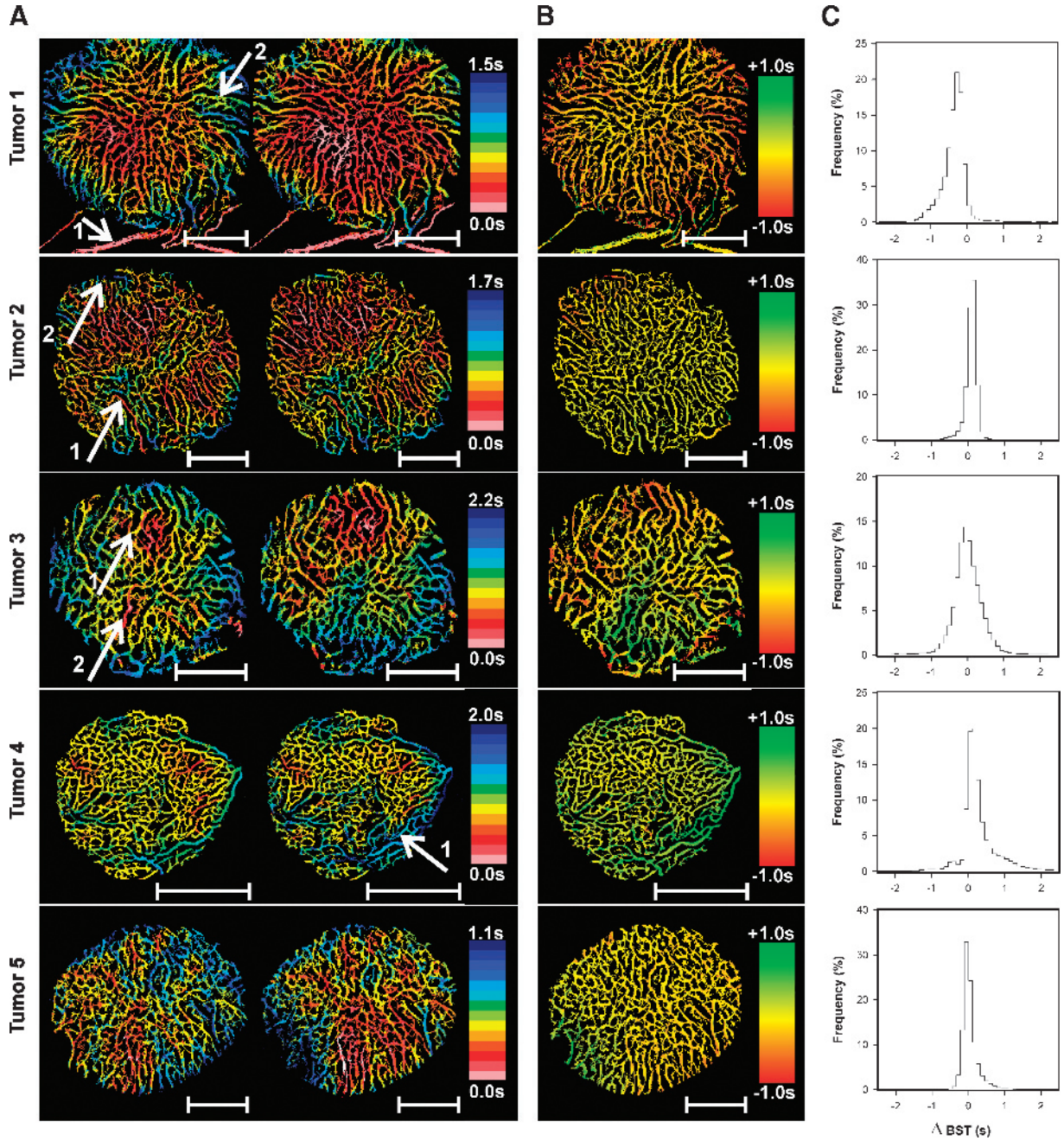

Figure 5. Five A-07-GFP window chamber tumors were subjected to BST imaging thrice. Each tumor is represented with two subsequent BST images (A) and the corresponding ΔBST image (B) and ΔBST frequency distribution (C). Identical color scales were used for the two BST images of a given tumor, thus highlighting the changes in BST occurring between the imaging series. Image regions of particular interest (described in detail in the Results section) are indicated by white arrows. Scale bars, 1 mm.

fluctuations in BST. Moreover, the BST fluctuations in different tumor subregions are independent of each other. In fact, it was observed that the BST in two different tumor subregions changed in opposite directions simultaneously, suggesting coordinated tumor blood supply redistribution.

To search for mechanisms leading to temporal heterogeneity in BST, high-resolution transmission microscopy imaging of individual tumor-supplying arteries and arterioles, tumor microvessels, and tumor-draining venules was performed. Instabilities in blood flow were observed in all vessel categories. Tumor microvessels could show total vascular stasis. The stases persisted for several seconds and were caused by arrest of circulating white blood cells in narrow microvascular passageways (Figure 6*A* and Supplementary movie 1). Tumor-draining venules were characterized by showing low blood flow velocities and could show abnormalities such as pulsating flow and even reversed flow direction, most likely caused by instabilities in the intravascular hydrostatic pressure (Figure 6*B* and Supplementary movie 2). Tumor microvessels, draining venules, and even arterioles could show sudden reductions in vessel diameter, possibly caused by mechanical pressure induced by proliferating tumor cells, as illustrated for a tumor arteriole in Figure 6*C*. Tumor arteries and arterioles could show fluctuations in vessel diameter consistent with

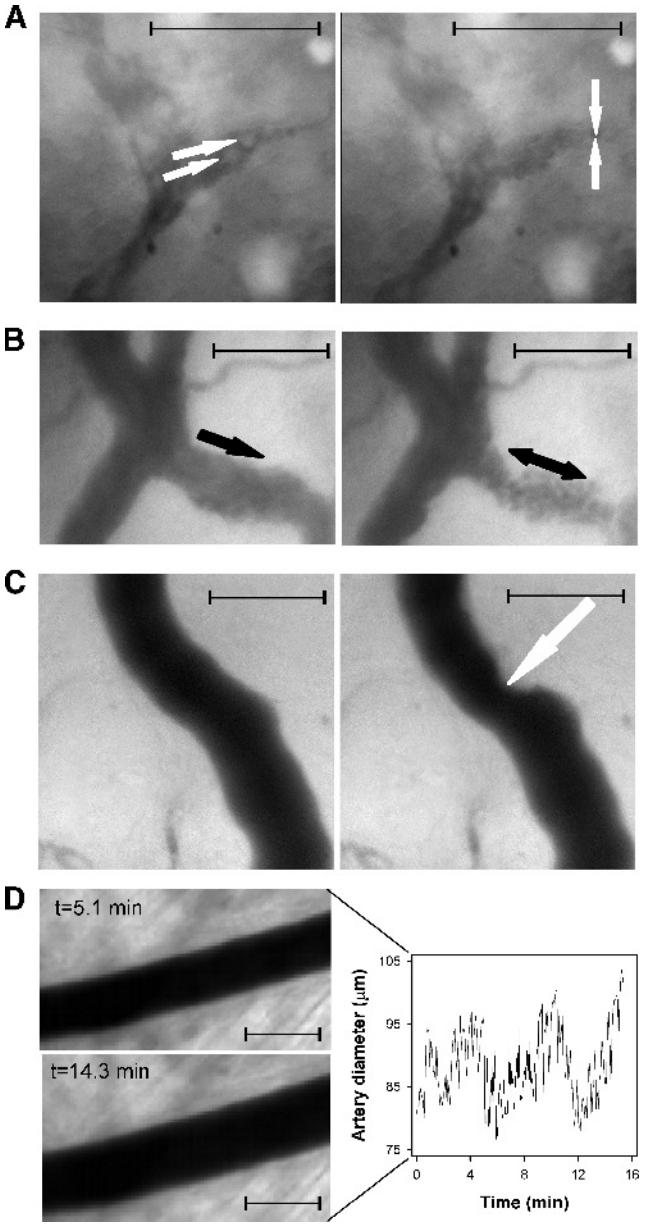

Figure 6. Four vessels in A-07-GFP window chamber preparations subjected to high magnification transmission microscopy imaging. (A) Two frames from a movie of a tumor microvessel. Two leukocytes (white arrows) approach a narrow passageway in the vessel (left). Shortly afterward, the leukocytes are trapped in the vessel and cause vascular stasis (right). The stasis lasted for a few seconds before the vessel reopened and the blood flow resumed (Supplementary movie 1). (B) Two frames from a movie of a tumor venule (black arrow). The blood flows orderly and unalterably through the vessel (left), and a few seconds later, the blood flow stops, pulsates, and becomes reversed (right). These blood flow abnormalities lasted for several seconds (Supplementary movie 2). (C) Two frames from a movie of a tumor-supplying arteriole showing the vessel before (left) and after (right) it is compressed. The compression lasted for ~75 seconds, and the vessel diameter at the site of compression (white arrow) was reduced to ~65% of its original value. (D) Two frames from a movie of a tumor-supplying artery showing arterial vasomotion (left) and a plot of artery diameter *versus* time (right). Maximum and minimum diameters differed by ~30% during the 16-minute observation period. The images presented in this figure were not derived from the same tumor. Scale bars, 100 μm in all images.

vasomotor activity, as illustrated for a tumor-supplying artery in Figure 6*D*. Tumor 1 showed a single supplying arteriole, and vasomotor activity in this arteriole changed the BST image of the tumor substantially (Figure 5, *upper row*).

Discussion

Several experimental methods have been used to demonstrate temporal instabilities in blood perfusion in experimental tumors, including laser Doppler techniques, T_2*-weighted magnetic resonance imaging, and dynamic contrast-enhanced magnetic resonance imaging [10–12]. In addition, intravital microscopy techniques have been used to measure temporal instabilities in red blood cell flux in individual vessels in small subregions of tumors growing in window chambers [13]. In the present study, temporal heterogeneities in blood flow velocity within the vasculature of window chamber tumors were visualized by repeated BST imaging. This is a novel imaging method that has significant advantages compared with the methods used previously for studying temporal heterogeneities in tumor blood flow. The main advantage is that the entire vascular network of tumors and the surrounding normal tissue can be examined simultaneously at high spatial resolution in a single imaging sequence.

The BST imaging was performed at a spatial resolution of 10.8 × 10.8 μm. Conflicting interests have to be taken into consideration when determining the optimal spatial resolution for BST imaging. Thus, high spatial resolution is desirable to allow clear and correct delineation of the tumor microvasculature. However, high spatial resolution results in small pixels and low signals, and consequently, at high spatial resolution, the signal-to-noise ratio may be too low to allow accurate BST calculations. The spatial resolution used here was sufficiently high to allow identification of the majority of the tumor vessels at the same time as the BST values of the vessels could be computed with high accuracy and reproducibility.

Blood supply time values were computed by using a tumor-supplying artery as reference vessel. To make it possible to identify comparable reference vessels in different window chamber preparations, the tumor-initiating spheroids were implanted in approximately the same position relative to the preexisting vascular network in all chambers. Thus, it was also ensured that the intertumor heterogeneity in BST observed here was not a consequence of differences in implantation site.

Attempts were made to keep the physiological conditions of the mice constant during and between the imaging series to avoid detection of artificial BST changes caused by changes in systemic factors such as blood pressure, body core temperature, and depth of anesthesia. We have shown that the blood perfusion in A-07 tumors is not altered by the anesthesia used in the present experiments as long as the body core temperature of the mice is maintained at a physiologically normal level [12]. Thus, a thermostatically controlled hot air generator was used to keep the mouse body core temperature between 37 and 38°C during the experiments. Moreover, the volume of the TRITC-dextran boluses was minimized to avoid perturbing the systemic blood pressure. To examine whether the physiological conditions of the mice had changed during an experiment, the plasma flow velocity in the reference vessel was measured retrospectively. Because the plasma flow velocity was found to be equal in the three imaging series, the temporal heterogeneities in BST observed here were biologically relevant heterogeneities and not artifacts caused by inappropriate experimental conditions.

Three main types of temporal heterogeneity in BST were observed, and the underlying mechanisms were not necessarily the same. First, global and homogeneous changes in BST (i.e., similar changes in the entire vascular network) were seen in one of the five tumors, and this tumor was supplied by a single arteriole. Because the causes of BST changes are likely to be found upstream of the site of the changes, the BST changes in this tumor were probably induced by the tumor-supplying arteriole. Previous studies have revealed that vasomotor activity can provoke extensive changes in the diameter of tumor-feeding vessels [13]. Vasomotion in afferent arterioles is associated with complex fluctuation patterns, and it has been observed that arteriolar vasomotion correlates well with temporal heterogeneities in tumor blood flow and oxygen tension [13]. Our study confirmed that vasomotor activity can occur in tumor-supplying vessels, and for tumors having only one feeding arteriole, the downstream effects of arteriolar vasomotion are expected to be extensive. Taken together, our observations suggest that global and homogeneous changes in BST may occur in tumors having a single supplying arteriole and that these BST changes are caused by vasomotor activity in the supplying arteriole.

Second, regional changes in BST (i.e., homogeneous changes in BST within two or three subregions of tumors) were observed, and the BST changes in different tumor subregions were, in general, not coordinated. Blood supply time changes of this type occurred in tumors having two or three supplying arterioles and were most likely caused by temporally uncoordinated vasomotor activity in the tumor-supplying arterioles. However, complete or partial compression of a tumor-supplying arteriole, as illustrated in Figure 6*C*, may also lead to regional changes in BST. It has been suggested that increased mechanical pressure induced by active tumor cell proliferation may cause such compressions [14].

Third, changes in BST in individual tumor vessel segments were observed. It is well known from several studies that the blood flow in tumor microvessels may show unstable velocity, intermittence, and regurgitation, a functional abnormality that most likely is a consequence of morphologic and architectural abnormalities in the vascular network [13]. Several mechanisms have been suggested, including microvessel compression caused by proliferating tumor cells [14] and microvessel obstruction caused by circulating tumor cells and/or leukocytes [13]. Our study demonstrated unequivocally that circulating leukocytes can cause intermittent obstructions in tumor microvessels (Figure 6*A*) and that the blood flow can pulsate and change direction in tumor venules (Figure 6*B*). Such incidents obviously cause BST changes in isolated vessel segments. However, the biologic consequences are probably modest compared with those generated by arteriolar vasomotor activity.

The BST images showed that the tumor tissue was supplied with blood from only one to three arterioles and thus experienced an inadequate arteriolar supply. This is not a unique feature of A-07-GFP window chamber tumors but a feature that A-07-GFP tumors have in common with many rodent and human tumors [1]. In tumors having a limited number of supplying arterioles, large tissue regions are supplied with blood from the same arteriole. Consequently, the erythrocytes may be depleted of oxygen on their way through the vascular network from the supplying arterioles to the tumor microvessels, giving rise to a phenomenon known as longitudinal P_{O_2} gradients [1]. It has thus been demonstrated that the intravessel oxyhemoglobin saturation is close to zero in large regions of many human and experimental tumors, including A-07 tumors [15–18], suggesting that the tumor tissue in these regions experiences hypoxia. Because the erythrocyte velocity is similar to or lower than the plasma velocity in tumor vessels [19], vessel segments showing high BST values have a high probability of carrying deoxygenated blood, and tumor tissue surrounding vessel segments having BST values above some threshold value has to be hypoxic, independent of the red blood cell flux [7]. The present observations that tumors may have a limited number of supplying arterioles and that the BST may fluctuate in large tumor regions because of vasomotion in the arterioles suggest that the development of hypoxic regions in tumor tissue is a highly complex and dynamic process. The commonly used distinction between diffusion-limited chronic hypoxia and perfusion-limited transient hypoxia is, therefore, too simplified to give an adequate description of the mechanisms leading to the development of hypoxia in tumors.

In summary, a novel method for mapping the spatial and temporal heterogeneity in blood supply in whole tumors growing in window chambers is reported, and studies of A-07-GFP tumors revealed that tumors can show significant heterogeneity in BST. The spatial heterogeneity is determined primarily by the number of tumor-supplying arterioles and their location in the tissue. The temporal heterogeneity can involve the entire tumor, tumor subregions, or single vessel segments and may be a consequence of vasomotor activity in the tumor-supplying arterioles, mechanical compression of vessel walls, and vessel obstruction caused by circulating white blood cells.

Acknowledgments

The authors thank Lars Aurdal at the Norwegian Computing Centre for participating in the software development, and Bjørn A. Graff in our research group for having recorded Supplementary movie 1.

References

[1] Dewhirst MW, Ong ET, Braun RD, Smith B, Klitzman B, Evans SM, and Wilson D (1999). Quantification of longitudinal tissue P_{O_2} gradients in window chamber tumours: impact on tumour hypoxia. *Br J Cancer* **79**, 1717–1722.

[2] Vaupel P, Kallinowski F, and Okunieff P (1989). Blood flow, oxygen and nutrient supply, and metabolic microenvironment of human tumors: a review. *Cancer Res* **49**, 6449–6465.

[3] Dewhirst MW, Ong ET, Klitzman B, Secomb TW, Vinuya RZ, Dodge R, Brizel D, and Gross JF (1992). Perivascular oxygen tensions in a transplantable mammary tumor growing in a dorsal flap window chamber. *Radiat Res* **130**, 171–182.

[4] Brown JM and Giaccia AJ (1998). The unique physiology of solid tumors: opportunities (and problems) for cancer therapy. *Cancer Res* **58**, 1408–1416.

[5] Höckel M and Vaupel P (2001). Tumor hypoxia: definitions and current clinical, biologic, and molecular aspects. *J Natl Cancer Inst* **93**, 266–276.

[6] Horsman MR (1995). Nicotinamide and other benzamide analogs as agents for overcoming hypoxic cell radiation resistance in tumours. A review. *Acta Oncol* **34**, 571–587.

[7] Øye KS, Gulati G, Graff BA, Gaustad JV, Brurberg KG, and Rofstad EK (2008). A novel method for mapping the heterogeneity in blood supply to normal and malignant tissues in the mouse dorsal window chamber. *Microvasc Res* **75**, 179–187.

[8] Gaustad JV, Brurberg KG, Simonsen TG, Mollatt CS, and Rofstad EK (2008). Tumor vascularity assessed by magnetic resonance imaging and intravital microscopy imaging. *Neoplasia* **10**, 354–362.

[9] Rofstad EK (1994). Orthotopic human melanoma xenograft model systems for studies of tumour angiogenesis, pathophysiology, treatment sensitivity and metastatic pattern. *Br J Cancer* **70**, 804–812.

[10] Braun RD, Lanzen JL, and Dewhirst MW (1999). Fourier analysis of fluctuations of oxygen tension and blood flow in R3230Ac tumors and muscle in rats. *Am J Physiol* **277**, H551–H568.

[11] Baudelet C, Ansiaux R, Jordan BF, Havaux X, Macq B, and Gallez B (2004). Physiological noise in murine solid tumours using T_2*-weighted gradient-echo imaging: a marker of tumour acute hypoxia? *Phys Med Biol* **49**, 3389–3411.

[12] Brurberg KG, Benjaminsen IC, Dørum LM, and Rofstad EK (2007). Fluctuations in tumor blood perfusion assessed by dynamic contrast-enhanced MRI. *Magn Reson Med* **58**, 473–481.

[13] Dewhirst MW, Kimura H, Rehmus SW, Braun RD, Papahadjopoulos D, Hong K, and Secomb TW (1996). Microvascular studies on the origins of perfusion-limited hypoxia. *Br J Cancer Suppl* **27**, S247–S251.

[14] Padera TP, Stoll BR, Tooredman JB, Capen D, di Tomaso E, and Jain RK (2004). Pathology: cancer cells compress intratumour vessels. *Nature* **427**, 695.

[15] Fenton BM, Rofstad EK, Degner FL, and Sutherland RM (1988). Cryospectrophotometric determination of tumor intravascular oxyhemoglobin saturations: dependence on vascular geometry and tumor growth. *J Natl Cancer Inst* **80**, 1612–1619.

[16] Måseide K, Lyng H, and Rofstad EK (2001). Microvessel oxyhemoglobin saturation does not reflect tissue oxygen tension in human melanoma xenografts. *Microvasc Res* **61**, 199–202.

[17] Rofstad EK, DeMuth P, Fenton BM, and Sutherland RM (1988). ^{31}P nuclear magnetic resonance spectroscopy studies of tumor energy metabolism and its relationship to intracapillary oxyhemoglobin saturation status and tumor hypoxia. *Cancer Res* **48**, 5440–5446.

[18] Måseide K and Rofstad EK (2001). Intratumour heterogeneity in microvessel oxyhaemoglobin saturations. *Cancer Lett* **162**, 245–251.

[19] Jain RK (1988). Determinants of tumor blood flow: a review. *Cancer Res* **48**, 2641–2658.